

A nonlinear analysis of the effect of heat transfer on capillary jet instability

Dipin S. Pillai, Prasanth Narayanan, S. Pushpavanam, T. Sundararajan, A. Jasmin Sudha et al.

Citation: *Phys. Fluids* **24**, 124106 (2012); doi: 10.1063/1.4772974

View online: <http://dx.doi.org/10.1063/1.4772974>

View Table of Contents: <http://pof.aip.org/resource/1/PHFLE6/v24/i12>

Published by the [American Institute of Physics](#).

Related Articles

Stability characteristics of solutocapillary Marangoni motion in evaporating thin films
Phys. Fluids **24**, 122104 (2012)

Bag instabilities
Phys. Fluids **24**, 091112 (2012)

Study of liquid jet instability by confocal microscopy
Rev. Sci. Instrum. **83**, 073104 (2012)

Buckling instability of squeezed droplets
Phys. Fluids **24**, 072102 (2012)

Thermocapillary instabilities in an evaporating drop deposited onto a heated substrate
Phys. Fluids **24**, 032103 (2012)

Additional information on Phys. Fluids

Journal Homepage: <http://pof.aip.org/>

Journal Information: http://pof.aip.org/about/about_the_journal

Top downloads: http://pof.aip.org/features/most_downloaded

Information for Authors: <http://pof.aip.org/authors>

ADVERTISEMENT



**Running in Circles Looking
for the Best Science Job?**

Search hundreds of exciting
new jobs each month!

<http://careers.physicstoday.org/jobs>

physicstoday JOBS



A nonlinear analysis of the effect of heat transfer on capillary jet instability

Dipin S. Pillai,¹ Prasanth Narayanan,¹ S. Pushpavanam,¹ T. Sundararajan,² A. Jasmin Sudha,³ and P. Chellapandi⁴

¹*Department of Chemical Engineering, Indian Institute of Technology Madras, Chennai 600036, India*

²*Department of Mechanical Engineering, Indian Institute of Technology Madras, Chennai 600036, India*

³*Safety Engineering Division, Indira Gandhi Centre for Atomic Research, Kalpakkam 603102, India*

⁴*Nuclear and Safety Engineering Group, Indira Gandhi Centre for Atomic Research, Kalpakkam 603102, India*

(Received 1 May 2012; accepted 3 December 2012; published online 28 December 2012)

Breakup of slender liquid jets under isothermal conditions has been studied extensively. In this work, we investigate the breakup of a viscous jet emanating from an orifice in the presence of convective heat transfer. We study the case where heat is transferred from the jet to the ambient fluid. The temperature varies axially and both viscosity and surface tension are taken to be temperature dependent. Marangoni stresses caused by a thermally induced surface tension gradient are included here. A numerical model based on a one-dimensional slender jet approximation of the equations of motion and heat transfer is used. This results in three coupled nonlinear partial differential equations, which are solved using the method of lines. The advantages of using this approximation lie in (i) its computational elegance and (ii) the physical insight that it provides. We compare the model predictions of both spatial and temporal stability analysis with experiments of a jet of molten Woods metal in water. Molten Woods metal emanating from various orifice diameters (1-10 mm) into water under the action of gravity is analysed for drop sizes and these are compared with the numerical predictions. The presence of heat transfer is found to shorten the breakup length of the jet. This is attributed to the increase in surface tension induced by the heat loss from jet to the ambient. It is found that including the effect of temperature dependence of viscosity and surface tension, however, does not affect the drop size. A critical dimensionless number ($\Pi_1 \sim 10$) is found to exist beyond which the breakup is dominated by Marangoni stresses. Below this critical number, the jet breaks up due to the combined effects of the capillary force and the Marangoni stresses. It is shown that including the effect of gravity is necessary to predict the drop size accurately. The results of this work have implications in evaluating safety strategies in the event of a core disruptive accident in a nuclear reactor. A wider application of this analysis is in improving the efficiency of thermally modulated inkjet printing. © 2012 American Institute of Physics. [<http://dx.doi.org/10.1063/1.4772974>]

I. INTRODUCTION

Breakup of a cylindrical liquid jet into small spherical drops is attributed to hydrodynamic instabilities driven by surface tension.¹ It was theoretically studied in this framework for the first time by Lord Rayleigh.² He analysed the temporal instability of the cylindrical base state of a stationary fluid and established that only axisymmetric disturbances with wavelengths larger than the undisturbed jet circumference grow in time. The maximum in the growth rate was found to occur at a wavenumber of $0.696/R_0$, where R_0 is the radius of the unperturbed stationary jet. The temporal

analysis of Rayleigh was extended to include the effects of viscosity by Weber³ and Chandrasekhar.⁴ Viscosity was found to have a dampening effect and lowered the growth rates. It was found that the fastest growing mode shifted to longer wavelengths thereby increasing the drop size. Tomotika⁵ studied the temporal stability of a viscous fluid cylinder in another viscous medium. He confined his analysis to the limiting case of negligible inertia of both fluids and obtained a dispersion relation for fluids with different viscosity ratios. Meister and Scheele⁶ presented the various limiting cases of Tomotika's analysis and also came up with numerical solutions to the generalised equation developed by Tomotika. Keller *et al.*⁷ observed that these theories were based on the assumption that the disturbances are temporally growing, while the perturbations actually grow in space in the direction of flow. In particular, they pointed out that the disturbance near the orifice never grew in time. They extended Rayleigh's analysis for spatially growing disturbances and found that Rayleigh's results are relevant only for the case of high Weber numbers (We). For low We (below a critical We) they found a new mode of faster growing disturbances of much larger wavelengths than those associated with the Rayleigh mode. This mode was related to an absolute instability by Leib and Goldstein.⁸ A generalized spatiotemporal analysis is needed to predict absolute instabilities. Absolute instabilities have never been observed in the presence of gravity.⁹ They have been reported only in microgravity¹⁰ or in horizontal flows.⁹ The focus of this work is therefore only on convective instabilities, as we study vertical jets.

In this study, we use the slender jet approximation of governing equations.¹ Eggers and Dupont¹¹ used this to study dripping from a faucet. Furlani *et al.*¹² used these equations to study temporal stability in the presence of surface tension gradients and predicted the breakup of microjets. They incorporated thermal modulation of the jet by directly varying surface tension without solving the energy equation. Cheong *et al.*¹³ used the slender jet equations to study the effect of gravity on the breakup of jet. All the above analysis were carried out for isothermal jets. Furlani *et al.*^{14–16} have used the slender jet analysis to study the effect of thermal modulation on jet breakup with applications in inkjet printing. However, they have not extensively discussed the effects of convective heat transfer (from the jet to the ambient) on jet breakup. In this paper, we study the effect of heat transfer on the breakup of a jet. The effect of thermally induced variation in surface tension and viscosity is considered by solving the slender jet form of the energy equation. This investigation assumes significance in the event of a core-disruptive accident (CDA) in a nuclear reactor. The breakup of jet of molten nuclear core (called corium) in the coolant during a severe accident is expected to be different from what has been studied under isothermal conditions. The corium loses heat along its axial length as it moves, causing axial gradients in surface tension and viscosity. To the best of our knowledge, no study on jet breakup has been reported which takes into consideration the effect of both surface tension and viscosity variation along the axial length of the jet, induced by convective heat transfer.

In the event of a CDA in a fast breeder reactor (FBR), it is envisaged that jets of molten corium while losing heat to the coolant will break up into droplets as they move down in the coolant due to interfacial instabilities.¹⁷ The study of the interactions of a molten nuclear fuel with the coolant inside a nuclear reactor is called molten fuel coolant interaction (MFCI). Several MFCI experiments with molten fuel in sodium have been reported in literature. However, a convenient and safe way to study MFCI is to study the fuel-coolant interactions with simulant materials. There are several studies analysing Woods metal-water interaction as a suitable simulant system for a MFCI in a FBR.^{17–21} Bang *et al.*²⁰ reported that the breakup of a pressure-driven jet of Woods metal in water is governed by Kelvin-Helmholtz instability. They attributed this to the sufficiently high relative velocity between the jet and the ambient fluid. However, in a freely falling jet under the influence of gravity the relative velocities between the fluids are low. Here, the Rayleigh-plateau instability drives the jet breakup.

The primary objective of any containment strategy in a CDA is to ensure that the resultant debris is fine enough to completely solidify at the reactor bottom. This happens when the growth rates of hydrodynamic instabilities (that breakup the jet) are higher than the solidification rate. The present study aims at studying MFCI as a simplified case of jet breakup due to hydrodynamic instabilities in the presence of heat transfer. In this work, we restrict our focus on the breakup of jet wherein the growth rate of instabilities is higher than the rate of solidification.

In Sec. II, we derive the governing equations (conservation of mass, momentum, and energy) using the slender jet approximation. In Sec. III, details of the various simulations performed are described. In Sec. IV, we describe the experimental setup and procedure. Section V discusses the results and Sec. VI presents the conclusions of our study.

II. THEORETICAL ANALYSIS

In this section, we discuss the equations of motion and energy and the boundary conditions governing the breakup of an axisymmetric viscous jet of an incompressible Newtonian fluid with density ρ , surface tension σ , viscosity μ , temperature T , thermal conductivity k_t , heat capacity C_p in an immiscible inviscid fluid maintained at a lower temperature T_c (Fig. 1). We take into account the effect of gravity and Marangoni stresses by allowing the surface tension to vary with temperature. Effect of variations in viscosity with temperature is also taken into account. This can be important when the jet undergoes solidification due to heat transfer to the ambient. Since the fluids are immiscible, no mass transfer across the interface occurs. As the jet is taken to be axisymmetric, we neglect any variations in the azimuthal direction. We take z as the axial and r as the radial direction.

A. Governing equations

The equation of continuity or mass conservation is given by

$$\frac{1}{r} \frac{\partial}{\partial r} (ru_r) + \frac{\partial u_z}{\partial z} = 0. \quad (1)$$

Subscripts r and z refer to the radial and axial components, respectively. The equations of motion of a fluid with variable viscosity are given by the modified Navier-Stokes equation

$$\begin{aligned} & \frac{\partial u_z}{\partial t} + u_r \frac{\partial u_z}{\partial r} + u_z \frac{\partial u_z}{\partial z} \\ &= -\frac{1}{\rho} \frac{\partial p}{\partial z} + \nu \left[\frac{1}{r} \frac{\partial}{\partial r} \left(r \frac{\partial u_z}{\partial r} \right) + \frac{\partial^2 u_z}{\partial z^2} \right] + \frac{2}{\rho} \frac{\partial u_z}{\partial z} \frac{\partial \mu}{\partial z} + \frac{1}{\rho} \left(\frac{\partial u_z}{\partial r} + \frac{\partial u_r}{\partial z} \right) \frac{\partial \mu}{\partial r} + g, \quad (2) \end{aligned}$$

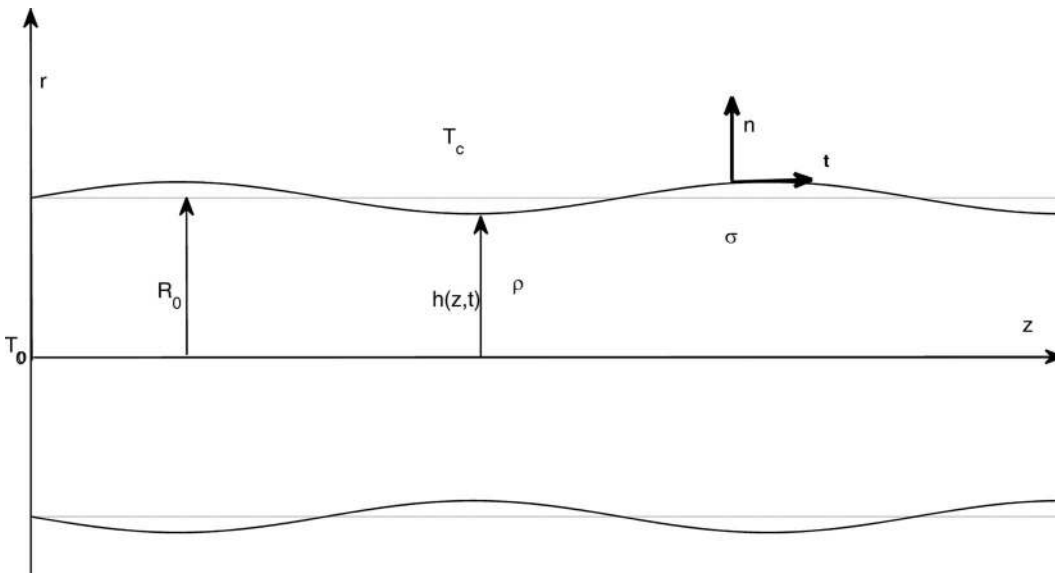


FIG. 1. Schematic of a semi-infinite jet emanating from an orifice.

$$\begin{aligned} & \frac{\partial u_r}{\partial t} + u_r \frac{\partial u_r}{\partial r} + u_z \frac{\partial u_r}{\partial z} \\ &= -\frac{1}{\rho} \frac{\partial p}{\partial r} + \nu \left[\frac{\partial}{\partial r} \left(\frac{1}{r} \frac{\partial}{\partial r} (r u_r) \right) + \frac{\partial^2 u_r}{\partial z^2} \right] + \frac{2}{\rho} \frac{\partial u_r}{\partial r} \frac{\partial \mu}{\partial r} + \frac{1}{\rho} \left(\frac{\partial u_z}{\partial r} + \frac{\partial u_r}{\partial z} \right) \frac{\partial \mu}{\partial z}. \end{aligned} \quad (3)$$

Here, $\nu = \mu/\rho$ is the kinematic viscosity and g is the acceleration due to gravity. We have assumed the fluid to be incompressible (density is assumed to be independent of temperature) but have retained the viscosity dependence on temperature. The gravity vector is assumed to act along the flow, i.e., z direction.

The energy equation is given by

$$\frac{\partial T}{\partial t} + u_r \frac{\partial T}{\partial r} + u_z \frac{\partial T}{\partial z} = \frac{k_t}{\rho C_p} \left[\frac{1}{r} \frac{\partial}{\partial r} \left(r \frac{\partial T}{\partial r} \right) + \frac{\partial^2 T}{\partial z^2} \right]. \quad (4)$$

B. Boundary conditions

Let the position of the jet interface shown in Fig. 1 be described by a surface $f(r, z, t)$ such that

$$f(r, z, t) \equiv r - h(z, t) = 0. \quad (5)$$

The kinematic boundary condition is given by

$$u_r = \frac{\partial h}{\partial t} + u_z \frac{\partial h}{\partial z} \quad \text{at } r = h. \quad (6)$$

At the interface, the normal and tangential stress conditions are given by

$$\begin{aligned} p + \frac{2\mu}{1 + \left(\frac{\partial h}{\partial z}\right)^2} \left[\frac{\partial h}{\partial z} \left(\frac{\partial u_r}{\partial z} + \frac{\partial u_z}{\partial r} \right) - \frac{\partial u_z}{\partial z} \left(\frac{\partial h}{\partial z} \right)^2 - \frac{\partial u_r}{\partial r} \right] - p_a \\ = \frac{\sigma}{\sqrt{1 + \left(\frac{\partial h}{\partial z}\right)^2}} \left[\frac{1}{h} - \frac{\frac{\partial^2 h}{\partial z^2}}{1 + \left(\frac{\partial h}{\partial z}\right)^2} \right], \end{aligned} \quad (7)$$

$$\frac{\mu}{1 + \left(\frac{\partial h}{\partial z}\right)^2} \left[2 \frac{\partial h}{\partial z} \left(\frac{\partial u_r}{\partial r} - \frac{\partial u_z}{\partial z} \right) + \left(\frac{\partial u_r}{\partial z} + \frac{\partial u_z}{\partial r} \right) \left(1 - \left(\frac{\partial h}{\partial z}\right)^2 \right) \right] = \frac{\left(\frac{\partial \sigma}{\partial z} + \frac{\partial \sigma}{\partial r} \frac{\partial h}{\partial z} \right)}{\sqrt{1 + \left(\frac{\partial h}{\partial z}\right)^2}} \quad \text{at } r = h. \quad (8)$$

Here, the ambient fluid is assumed to be inviscid and its pressure, p_a , is assumed to be uniform.

At the interface, the diffusional rate of heat transfer in the normal direction is equal to the convective rate of heat transfer. If the heat transfer coefficient is given by h_{tr} , then we get

$$\frac{-k_t}{\sqrt{1 + \left(\frac{\partial h}{\partial z}\right)^2}} \left(\frac{\partial T}{\partial r} - \frac{\partial h}{\partial z} \frac{\partial T}{\partial z} \right) = h_{tr} (T - T_c) \quad \text{at } r = h. \quad (9)$$

C. Method of solution

The governing equations along with the boundary conditions are solved using the slender jet approximation.^{11,12} Here, when the dimensions of the jet are such that its length is much greater than its radius ($L \gg R_0$), the dependent variables velocity, pressure, and temperature anywhere

along the jet can be written as a series expansion in the radial coordinate. In our simulations, L is 50–100 times R_0 . Woods metal (9383 kg/m^3) is significantly denser than water (1000 kg/m^3) and the surface tension of the system is 1 N/m . Our analysis retains the effect of surface tension but assumes the coolant to be inviscid. The characteristic velocity (U_c) when the inertial and capillary forces are balanced is therefore low compared to the inlet velocity (U_0). For a 10 mm orifice, it is found that $U_c \sim \frac{1}{5}U_0$. Under these conditions the linearized slender jet approximation provides reliable estimates of breakup times.¹⁵ Thus, the slender jet approximation for this study is justified based on the surface tension and densities of the Woods metal and water system.

The axial velocity component, pressure, and temperature are approximated as power series in the radial direction about the axis of the jet. However, since the variables are symmetric about $r = 0$, the first derivative of the variables with respect to r vanishes at $r = 0$ and we obtain

$$\begin{aligned} u_z(r, z, t) &= u_0(z, t) + r^2 u_2(z, t) + \dots, \\ p(r, z, t) &= p_0(z, t) + r^2 p_2(z, t) + \dots, \\ T(r, z, t) &= T_0(z, t) + r^2 T_2(z, t) + \dots \end{aligned} \quad (10)$$

Substituting the above variables in the governing equations (Sec. II A) along with the boundary conditions (Sec. II B), we obtain the slender jet equations as follows:

$$\frac{\partial u_0}{\partial t} = -u_0 \frac{\partial u_0}{\partial z} - \frac{1}{\rho} \frac{\partial}{\partial z}(\sigma H) + \frac{2}{\rho h} \frac{\partial \sigma}{\partial z} + \frac{3\mu}{\rho h^2} \frac{\partial}{\partial z} \left(h^2 \frac{\partial u_0}{\partial z} \right) + \frac{3}{\rho} \frac{\partial \mu}{\partial z} \frac{\partial u_0}{\partial z} + g, \quad (11)$$

$$\frac{\partial h}{\partial t} = - \left(\frac{h}{2} \frac{\partial u_0}{\partial z} + u_0 \frac{\partial h}{\partial z} \right), \quad (12)$$

$$\frac{\partial T_0}{\partial t} = -u_0 \frac{\partial T_0}{\partial z} + \frac{k_t}{\rho C_p} \left[\frac{2}{h} \frac{\partial T_0}{\partial z} \frac{\partial h}{\partial z} - \frac{2h_{tr}}{k_t h} (T_0 - T_c) + \frac{\partial^2 T_0}{\partial z^2} \right]. \quad (13)$$

An important contribution of this work is the inclusion of the energy balance using the slender jet approximation to study how heat transfer affects the jet breakup. Effect of this convective heat transfer on the breakup dynamics (breakup times, lengths, and drop diameters) has not been reported in literature to the best of our knowledge.

We now describe the solution methodology based on the method of lines to solve for u_0 , h , and T_0 given by Eqs. (11), (12), and (13).

D. Numerical procedure

The slender jet equations [Eqs. (11), (12), and (13)] are simultaneously solved using the method of lines.¹² A uniform staggered grid is used along the axial length of the jet and the spatial derivatives are discretized using a central difference on these nodes. The partial differential equations of u_0 , T_0 , and h are thus converted into ordinary differential equations in time at each node. The ordinary differential equations for each of the nodal variables are solved in MATLAB2011a using the ode23t solver. The number of h nodes used for each of the simulations is 1200. It was verified that this number of nodes ensured grid independence. An increase in the number of nodes even up to 7000 changed the results only by 0.02%. The simulation was stopped when the interface position (h) reached 0.05 times the initial unperturbed radius. This was taken to be indicative of the jet breakup. All simulations are carried out for a range of orifice diameters, viz., 1, 2, 3, 5, 7, and 10 mm.

III. STABILITY ANALYSIS

In this work, we study the breakup of a vertical jet falling under gravity with heat being lost from jet to the ambient. Absolute instabilities have never been observed in jets in the presence of

gravity.⁹ Hence, the focus of this work is only on convective instabilities. To understand this, the nonlinear slender jet equations (Eqs. (11), (12), and (13)) are directly simulated. To understand the effect of heat transfer on jet breakup we compare the behaviour of isothermal and non-isothermal systems. While investigating the effect of heat transfer, however, we neglect gravity to solely focus on the effect of heat transfer on the dynamics of jet breakup. To analyse the effect of gravity on jet breakup we focus on isothermal jets. The effect of heat transfer on horizontal jets and gravity on isothermal jets helps us understand how various parameters critically affect the dynamics of jet breakup.

A. Isothermal temporal analysis—Horizontal jet

In temporal analysis, a sinusoidal perturbation is imposed on the interface throughout the length of the jet as an initial condition. The evolution of perturbation with time is followed to determine the breakup dynamics of the jet into drops. Since our interest is in the temporal evolution of a spatially periodic perturbation, we focus on the evolution of the perturbation for only one wavelength. The velocity of the jet is maintained zero initially in this domain. It is important to note that in isothermal simulations, we do not solve for temperature given by Eq. (13). Thus, we solve for h and u_0 , with the initial conditions

$$h(z, 0) = R_0 \left[1 + \varepsilon \cos \left(\frac{kz}{R_0} \right) \right], \quad u_0(z, 0) = 0, \quad (14)$$

where ε is 0.05 and k is the wavenumber of perturbation. R_0 is the radius of the orifice.

The length of the computational domain, L , that is solved for is one wavelength of perturbation since the profile is periodic along the length of the jet. The periodic boundary conditions imposed on the boundaries of the computational domain are

$$\begin{aligned} h(0, t) &= h(L, t), & u_0(0, t) &= u_0(L, t), \\ \frac{\partial h}{\partial z}(0, t) &= \frac{\partial h}{\partial z}(L, t), & \frac{\partial u_0}{\partial z}(0, t) &= \frac{\partial u_0}{\partial z}(L, t), \\ \frac{\partial^2 h}{\partial z^2}(0, t) &= \frac{\partial^2 h}{\partial z^2}(L, t). \end{aligned} \quad (15)$$

B. Isothermal spatial analysis—Horizontal jet

In spatial analysis, a sinusoidal perturbation with time is imposed on the velocity at the inlet. The perturbation is carried downstream along with the jet. It grows spatially and eventually breaks the jet into drops. Thus, our initial conditions are

$$h(z, 0) = R_0, \quad u_0(z, 0) = U_0, \quad (16)$$

where U_0 is the velocity of the jet at the inlet (0.5 m/s). The velocity of jet was obtained from the ratio of the average volumetric flow of Woods metal to the area of cross section of the orifice. The boundary conditions are

$$\begin{aligned} h(0, t) &= R_0, & u_0(0, t) &= U_0 \left[1 + \varepsilon \sin \left(\frac{\omega U_0 t}{R_0} \right) \right], \\ \frac{\partial h}{\partial z}(L, t) &= 0, & \frac{\partial u_0}{\partial z}(L, t) &= 0, \\ \frac{\partial^2 h}{\partial z^2}(L, t) &= 0, \end{aligned} \quad (17)$$

where ω is the frequency of oscillation of perturbation and ε is chosen as 0.05. The length of the computational domain, L , used for all simulations in spatial analysis is 50 times R_0 , unless specified otherwise. Several earlier works have numerically analysed the breakup of isothermal jets using

temporal and spatial analysis. The breakup times predicted by our model agree with those reported in the literature.¹²

C. Isothermal spatial analysis with gravity

When the jet moves vertically downward, gravity accelerates the jet. This causes a thinning of the jet along its axial length. This can result in lower drop sizes at breakup since the thinning can be viewed equivalent to a jet emanating from a reduced orifice diameter. The initial jet profile is assumed to be a thinning cylinder due to gravitational acceleration and is given as¹³

$$h(z, 0) = R_0 \left(1 + \frac{2gz}{U_0^2}\right)^{-1/4}, \quad u_0(z, 0) = U_0 \left(1 + \frac{2gz}{U_0^2}\right)^{1/2}. \quad (18)$$

Here a spatial stability analysis is carried out using the boundary conditions described in Sec. III B. It was observed that for larger orifice diameters, the breakup length was more than 50 times R_0 and therefore the simulations did not show breakup when the length of the computational domain (L) was retained at its default value of 50 times R_0 . Hence, these simulations are run with higher L values. For simulations of orifice diameters 5 mm and larger, L is fixed at 100 times R_0 .

D. Non-isothermal spatial analysis—Horizontal jet

In the non-isothermal spatial analysis, we include the effect of heat transfer between the jet and the ambient fluid. The jet leaves the orifice at a temperature T_{in} (373 K, which is the inlet temperature of Woods metal in experiments) and the ambient fluid is maintained at a constant lower temperature T_c (308 K). In non-isothermal simulations, we solve the additional equation for temperature T_0 [Eq. (13)] along with h and u_0 .

1. Temperature dependent surface tension

Heat transfer from the jet to the ambient fluid induces an axial variation of temperature. This causes the surface tension to vary along the surface and thus affects the jet breakup dynamics. Since, the breakup of jet is governed primarily by the capillary effect of surface tension, the variation in surface tension with temperature can have a significant effect on the breakup dynamics. We take surface tension to be a linear function of temperature,

$$\sigma = \sigma_0 - \beta(T - T_{ref}), \quad (19)$$

where $\sigma_0 = 1$ N/m is the surface tension at T_{ref} , 373 K, and $\beta = 0.01$ N/mK. The value of β for Woods metal is not known. Its value of β is assumed to be of the same order of magnitude as that of molten lead since it forms a major constituent of Woods metal. The temperature dependence of surface tension for lead has been experimentally determined by Passerone *et al.*²² and β is chosen to have the same order of magnitude.

The initial conditions and boundary conditions for u_0 and h remain the same as described in Sec. III B. The initial condition for T_0 is

$$T_0(z, 0) = T_{in} \quad (20)$$

and the boundary conditions for T_0 are

$$T_0(0, t) = T_{in}, \quad \frac{\partial T_0}{\partial z}(L, t) = 0. \quad (21)$$

The heat transfer coefficient given by Dittus-Boelter's correlation²³ is used in the analysis. The correlation is valid for fully turbulent flows. This correlation is used since Reynolds numbers are

very high for all the diameters. It varies between 1500 for 1 mm orifice diameter and 15 000 for 10 mm orifice diameter,

$$Nu_D = 0.023Re^{0.8} Pr^{0.3}. \quad (22)$$

Here, Re is the Reynolds number, Pr is the Prandtl number, and Nu_D is the Nusselt number defined as

$$Nu_D = h_{tr}D/k_t, \quad Re = \rho U_0 D/\mu, \quad Pr = \mu C_p/k_t, \quad (23)$$

where h_{tr} is the heat transfer coefficient, D is the unperturbed diameter of the jet, and k_t is the thermal conductivity of the jet. The heat transfer coefficient (h_{tr}) that appears in Eq. (13) is determined based on the Nusselt number obtained from Eq. (22).

2. Temperature dependent surface tension and viscosity

Since solidification takes place along with heat transfer, the variation of viscosity with temperature is expected to play an important role in determining the breakup behaviour. This is incorporated additionally by taking viscosity also to be a linear function of temperature as given by²⁴

$$\mu = \mu_0 - \alpha(T - T_{ref}), \quad (24)$$

where $\mu_0 = 0.0032 \text{ Ns/m}^2$, $\alpha = 1.03 \times 10^{-5} \text{ Ns/m}^2\text{K}$, and $T_{ref} = 353 \text{ K}$.

IV. EXPERIMENTAL ANALYSIS

The experimental apparatus consists of a furnace, a borosilicate glass funnel with a stand, and a cylindrical water tank made of Perspex. The diameter and the height of the tank are 240 mm and 600 mm, respectively. A schematic of the apparatus is shown in Fig. 2. The cylindrical perspex tank was filled with water up to a height of 550 mm while performing the experiments. Woods metal (50% Bi, 26.7% Pb, 13.3% Sn, 10% Cd by weight) in water has been used as a representative system to predict fuel coolant interactions in FBR.¹⁷⁻²¹ Properties of Woods metal are listed in Table I. About 550 g of Wood's metal (from Saru Smelting Ltd, Meerut, India) was heated to a temperature of 100 °C in a furnace. A funnel made of borosilicate glass was used to pour the molten Woods metal into the cylindrical tank. The mouth of the funnel was 1 cm below the water surface. Funnels of diameters 1 mm, 2 mm, 3 mm, 5 mm, 7 mm, and 10 mm were obtained from Logu Scientific Suppliers, Chennai, India. The funnels were also preheated to prevent any solidification and clogging of the funnel orifice. The coolant water was kept at room temperature. A high speed camera (X-PRI model, AOS Technologies) was used to capture the jet breakup at 1000 fps and the lighting was provided by two 80 W light emitting diode lamps (from Smart Energy Trade, Chennai, India). An iron stand was used to hold the funnel in place while pouring the Woods metal.

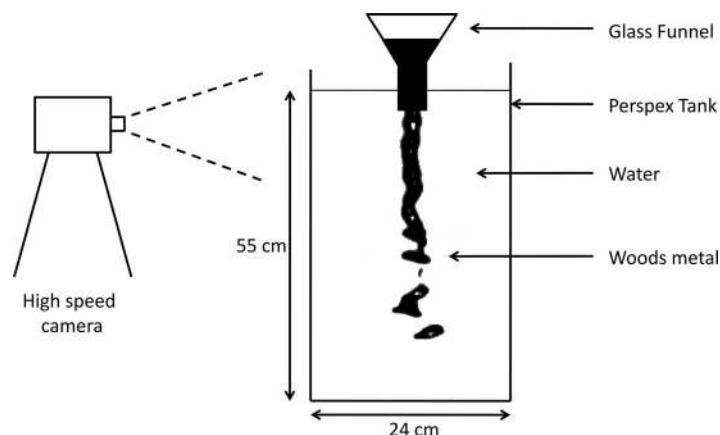


FIG. 2. Experimental setup for Wood's metal in water.

TABLE I. Properties of Woods metal (taken from Bang *et al.*²⁰).

Parameters	Values
Melting temperature	70 °C
Density	9383 kg/m ³
Specific heat	168 J/kg K
Thermal conductivity	18.8 W/m K
Kinematic viscosity	2×10^{-7} m ² /s
Surface tension	1 N/m

The molten metal flowed under the influence of gravity as a jet. The jet broke up and solidified to form debris. The debris was collected and dried before measuring the particle size distribution to determine the mass median diameter (MMD). Sieves (from A-1 Sieves and Screens, Chennai, India) with openings varying between 0.7 mm and 11 mm were used to determine the MMD. Experiments were repeated thrice for each orifice diameter to ensure repeatability.

V. RESULTS

The results from the experiments and the simulations are discussed in this section.

A. Experimental

The experiments were carried out using funnels with orifice diameters varying from 1 mm to 10 mm. It was found that for low orifice diameters, the debris were almost spherical in shape and of uniform size. They became irregular for larger orifice diameters. The debris collected for 1 mm and 5 mm orifice diameters are shown in Fig. 3. The irregularity in shape of the debris is attributed to the higher Weber numbers which prevail for larger orifice diameters. Here the inertial forces dominate over the capillary force, deforming the spherical interface.

The particle size distribution for different orifice diameters is shown in Fig. 4. For each of the orifice diameters, sieves with openings between 0.7 mm and 11 mm were used to obtain the particle size distribution. It was found that lower orifice diameters showed a narrower particle size distribution as compared to larger diameters (Fig. 4(a)). The spread in the particle size distribution for larger orifice diameters can be attributed to the experimentally observed secondary breakup of the drops. The distributions were used to determine the MMD.

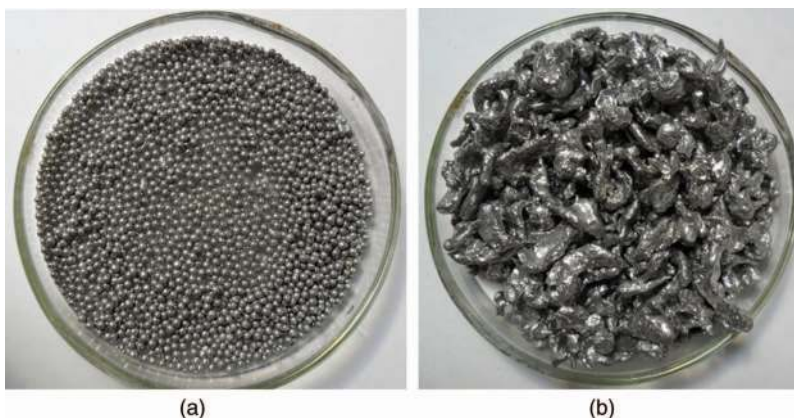


FIG. 3. Debris particles: (a) Spherical shape for 1 mm orifice diameter; (b) irregular shape for 5 mm orifice diameter.

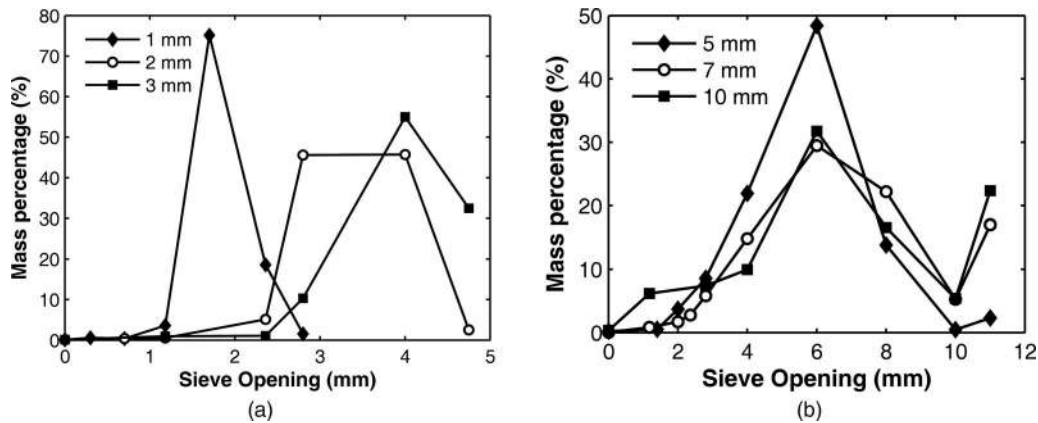


FIG. 4. (a) Particle size distributions for orifice diameters 1, 2, and 3 mm; (b) particle size distributions for orifice diameters 5, 7, and 10 mm.

The MMD obtained experimentally for different orifice diameters is shown in Fig. 5. It was observed that the experimentally obtained debris size (MMD) showed saturation as the orifice diameter increased. This can be explained based on (i) the thinning effect of gravity and (ii) the experimentally seen secondary breakup of the droplets. Small orifice diameters result in small primary drops that are held intact by surface tension. However, for larger orifice diameters, larger primary drops are formed, which are broken further into smaller drops due to the shearing effect of the ambient fluid as they travel down.

B. Isothermal temporal analysis—Horizontal jet

The simulations for temporal analysis were run for a range of wavelengths (k was varied from 0.05 to 1.5) and the critical wavelength (that which minimizes the breakup time) was determined as $k = 0.75$. It is expected that this critical wavelength would be the one that is seen experimentally as it grows the fastest among the naturally occurring disturbance frequencies.¹ Therefore, the results corresponding to this critical wavelength were used to determine the breakup characteristics. It was observed that the critical wavelength that minimizes the breakup time was independent of the orifice diameter. The interface profile at the time of pinch-off as predicted by a temporal stability analysis of Woods metal through a 1 mm diameter orifice is shown in Fig. 6.

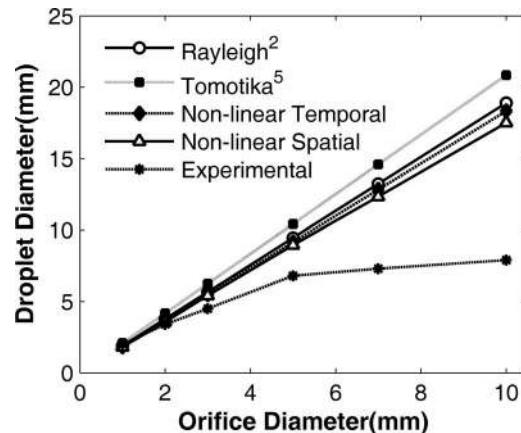


FIG. 5. Comparison of isothermal theoretical predictions of droplet diameter with the experimentally obtained mass median diameter for various orifice diameters.

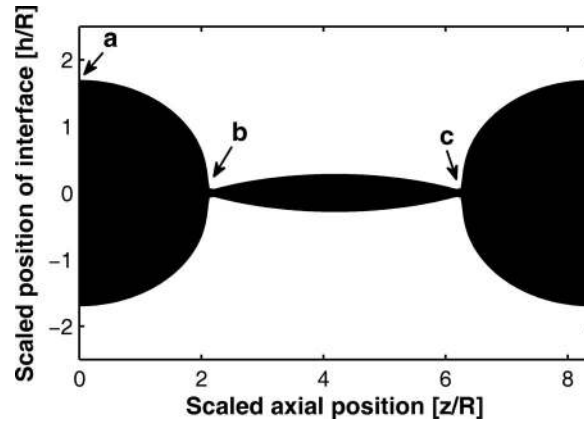


FIG. 6. Interface profile at the time of pinch-off (temporal analysis, 1 mm diameter).

The droplet volume was calculated using the disk integration method. The jet was treated as an effective cylindrical slug with a varying cross section. The volume between the limits of integration, *a* and *b*, marked in Fig. 6 is given by

$$V = \pi \int_a^b h^2 dz. \quad (25)$$

This volume corresponds to half a drop. Hence, the volume obtained above is doubled to determine the droplet volume V_d . The volume V_d thus obtained is considered to be an equivalent sphere and the droplet diameter is determined as

$$D_{drop} = 2 \left(\frac{3V_d}{4\pi} \right)^{1/3}. \quad (26)$$

The droplet diameter thus calculated from the nonlinear simulations was found to depend linearly on the orifice diameter (Fig. 5). The predictions based on linear stability theories of Rayleigh² and Tomotika⁵ also showed a similar trend for variation of drop diameter with orifice diameter. These are depicted in Fig. 5. These are not able to capture the experimentally observed saturation in MMD of drop size as orifice diameter increases.

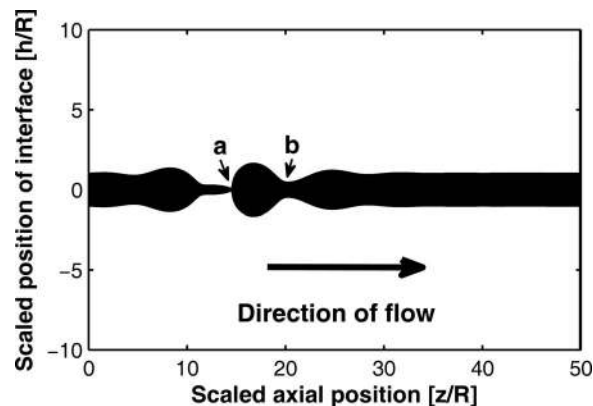


FIG. 7. Interface profile at the time of pinch-off (spatial analysis, 1 mm diameter).

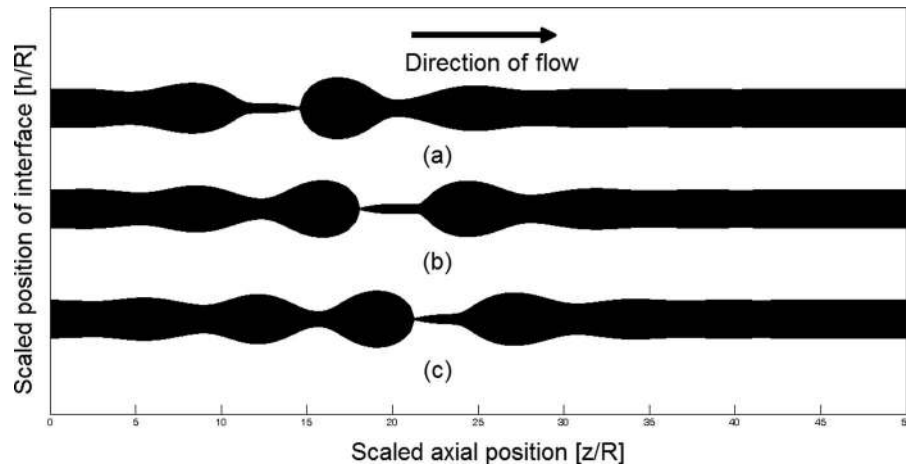


FIG. 8. Isothermal interface profile at the time of pinch-off (spatial analysis, horizontal jet) for different diameters: (a) 1 mm diameter, (b) 5 mm diameter, and (c) 10 mm diameter.

C. Isothermal spatial analysis—Horizontal jet

The simulations for spatial analysis were run for a range of frequencies (ω was varied from 0.05 to 1.5) and the critical frequency that minimizes the breakup time was determined ($\omega = 0.95$). It was again observed that this critical frequency remained the same for all orifice diameters. The results corresponding to this critical frequency were then used to determine the breakup characteristics.

The droplet diameter is calculated using the disk integration method described earlier. The limits of integration, a and b, for the spatial analysis are shown in Fig. 7. Point a is the point of pinch-off. The interface position attains a maximum value downstream of pinch-off and the position of the minimum immediately beyond this maximum value is point b. The volume so calculated gives the volume of the drop and it is equated to an equivalent sphere to determine the equivalent droplet diameter. The droplet diameter obtained by this approach again showed a linear variation with the orifice diameter (Fig. 5). Though, it was closer to the experimental results, this also did not show the experimentally observed saturation effect of particle size dependency on orifice diameter. Figure 8 shows the interface profile at the time of pinch-off for various orifice diameters as obtained using spatial analysis. It is seen that the breakup length increases with increasing orifice diameter.

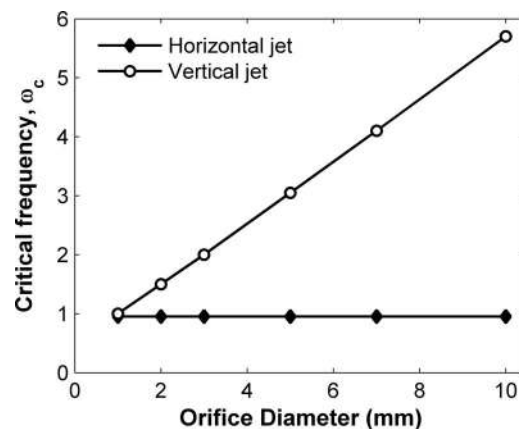


FIG. 9. Variation of critical frequency with orifice diameter (isothermal spatial analysis).

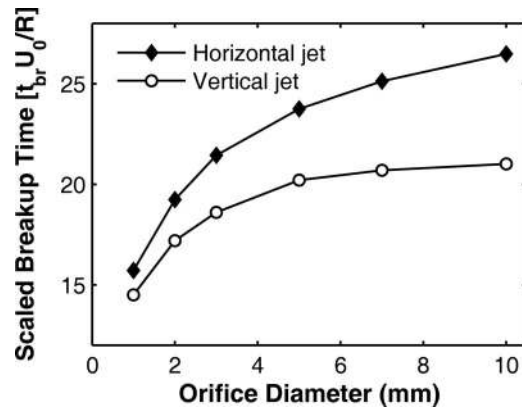


FIG. 10. Variation of jet breakup time with orifice diameter (isothermal spatial analysis).

D. Isothermal spatial analysis with gravity

The simulations for isothermal spatial analysis were run for a range of frequencies when the effect of gravity was included. The critical frequency that minimizes the breakup time was determined. Contrary to the case where the jet was horizontal, it was observed that the critical frequency increased with orifice diameters (Fig. 9). Also, the jet breakup times for the vertical jets were lower than those for the horizontal jets (Fig. 10).

On including gravity the breakup length was seen to increase due to the accelerating effect of gravity (compare Fig. 11 with Fig. 8). From Fig. 11 we see that the wavelength of perturbation on the interface that causes the breakup is shorter for larger orifice diameters. This is because the frequency of perturbation that causes the breakup is higher for larger diameters as is shown in Fig. 9.

The particle diameters obtained in this case are seen to be in better agreement and show a saturating effect similar to the experimentally observed results (Fig. 12). This saturating effect was not observed in the earlier analyses where gravity was not included. Thus, including the effect of gravity is important to predict the system behaviour accurately especially for larger orifice diameters.

E. Non-isothermal spatial analysis with thermally varying surface tension—Horizontal jet

We now focus on the analysis of the non-isothermal jet. The simulations for non-isothermal spatial analysis were run for a range of frequencies and the critical frequency that minimizes the

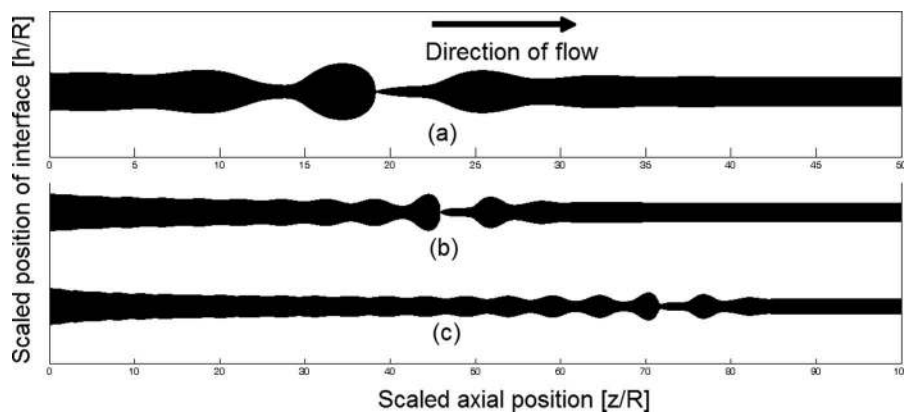


FIG. 11. Isothermal interface profile at the time of pinch-off (spatial analysis of jet with gravity) for different diameters: (a) 1 mm diameter, (b) 5 mm diameter, and (c) 10 mm diameter.

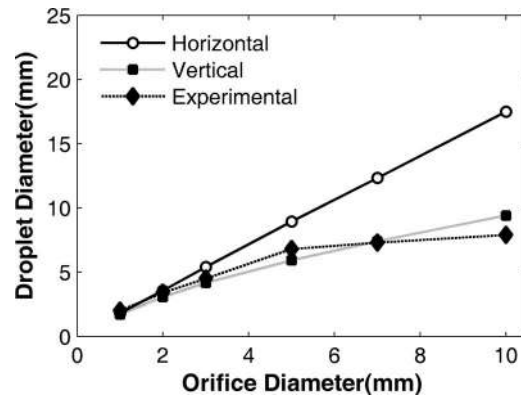


FIG. 12. Comparison of predictions of isothermal nonlinear spatial analysis of vertical and horizontal jets with experimentally obtained mass median diameter for various orifice diameters.

breakup time was determined. It was observed that the critical frequency did not vary with orifice diameters. Also, the critical frequency was found to be the same as that of the isothermal system (Fig. 13). Here, it can also be seen that in the presence of heat transfer, the breakup time decreases for all frequencies as compared to the isothermal case. This is expected because with heat transfer taking place from the jet to the ambient fluid, surface tension increases. Since jet breakup is driven by surface tension, this increases the breakup rate. Also, due to heat transfer, since a surface tension gradient is induced, an additional stress is induced by Marangoni effect leading to an accelerated breakup.

It is seen from Fig. 13 that for the non-isothermal case, even when the frequency of perturbation tends to zero (which essentially means no perturbation as we have assumed sinusoidal form for the perturbation), there is a finite breakup time. This fact was confirmed by imposing a zero amplitude perturbation at the inlet. The jet was again found to breakup with a finite breakup time. This is attributed to the fact that the additional Marangoni stress that sets in due to heat transfer can be viewed as a perturbation which grows spatially and breaks up the jet even in the absence of a disturbance at the inlet. It is seen that the low frequency disturbances also have a non-zero growth rate for a non-isothermal jet. This is as opposed to an isothermal jet which shows a large breakup time at low frequencies.

In Fig. 14 the jet breakup time for different values of the thermal sensitivity of surface tension (or β) is depicted. β is a measure of the extent of increase in surface tension with heat transfer. A higher β results in a larger variation of surface tension. Since jet breakup is driven by surface

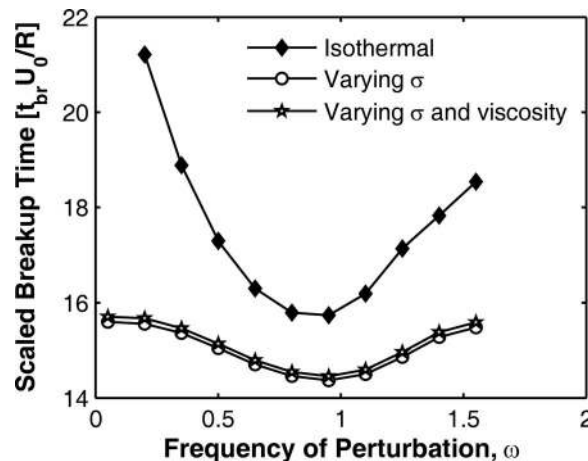


FIG. 13. Dependence of scaled breakup times on frequency of perturbation for isothermal and non-isothermal spatial analysis without gravity, $D = 1$ mm, $\beta = 0.001$ N m⁻¹ K⁻¹, $U_0 = 0.5$ ms⁻¹.

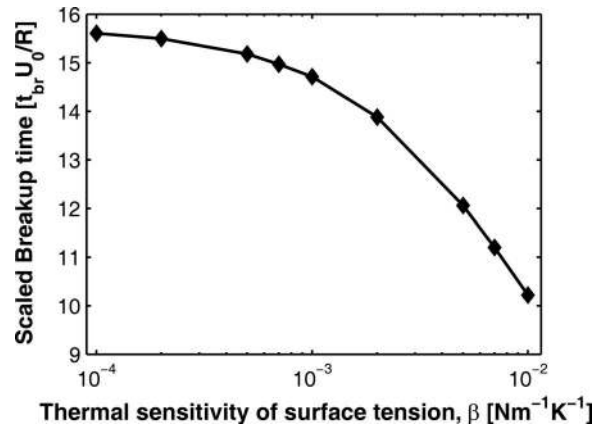


FIG. 14. Effect of thermal sensitivity of surface tension (β) on the jet breakup time, $D = 1$ mm.

tension, it results in lower breakup times. Consequently, we also see that the breakup length is smaller compared to the isothermal case (Fig. 15).

It was found that including heat transfer did not have any significant effect on the drop diameter. The minima or critical frequency in the dispersion curve remains the same in the presence of heat transfer. Since it is the critical frequency that grows spatially and determines the droplet diameter, this explains why the droplet diameter is not affected by the presence of heat transfer. This is in agreement with Rayleigh's linear analysis wherein it is found that the critical wavelength that grows the fastest is independent of the magnitude of surface tension. From his analysis, it is seen that surface tension affects the growth rate of all wavelengths; increasing (decreasing) the growth rates of all wavelengths for larger (smaller) surface tension. The breakup time in presence of heat transfer for a jet of Woods metal was determined as a function of the dimensionless group $\Pi_1 = \beta \frac{(T_m - T_c)}{\sigma_0}$. From Fig. 16, it is seen that there exists a critical $\Pi_1 \sim 10$ beyond which the breakup time is independent of Π_1 and depends solely on the absolute value of β . β is the sensitivity of surface tension to temperature and therefore a measure of the surface tension gradient. Thus, for large Π_1 , we see that the breakup time is determined solely by Marangoni stresses, while for lower Π_1 , it is the combined effect of capillary force and Marangoni stresses that determines the breakup time. In the latter region, we see an increase in breakup time with Π_1 . Simulations were performed for two different Re by changing the orifice diameter. The critical Π_1 beyond which the breakup time remains a constant was found to be independent of the Reynolds number.

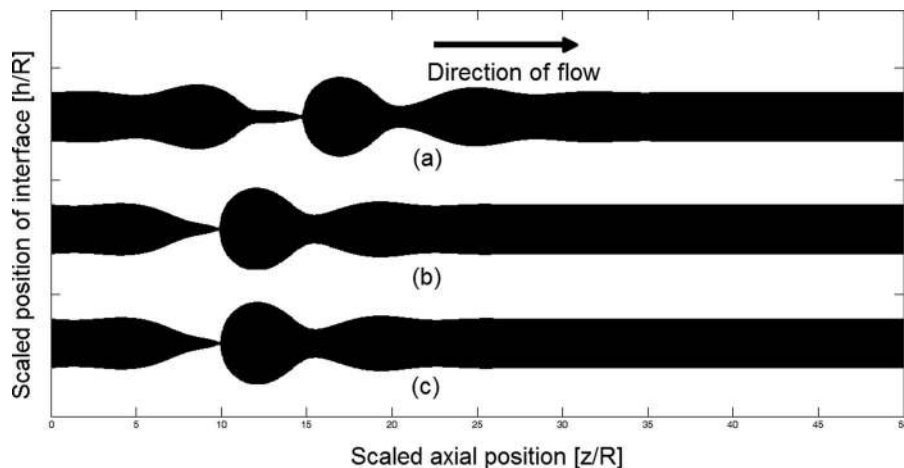


FIG. 15. Spatial analysis without gravity for 1 mm orifice diameter: (a) Isothermal; (b) thermally varying surface tension, $\beta = 0.01$ N/mK; (c) thermally varying surface tension and viscosity, $\beta = 0.01$ N/mK and $\alpha = 1.03 \times 10^{-5}$ Ns/m²K.

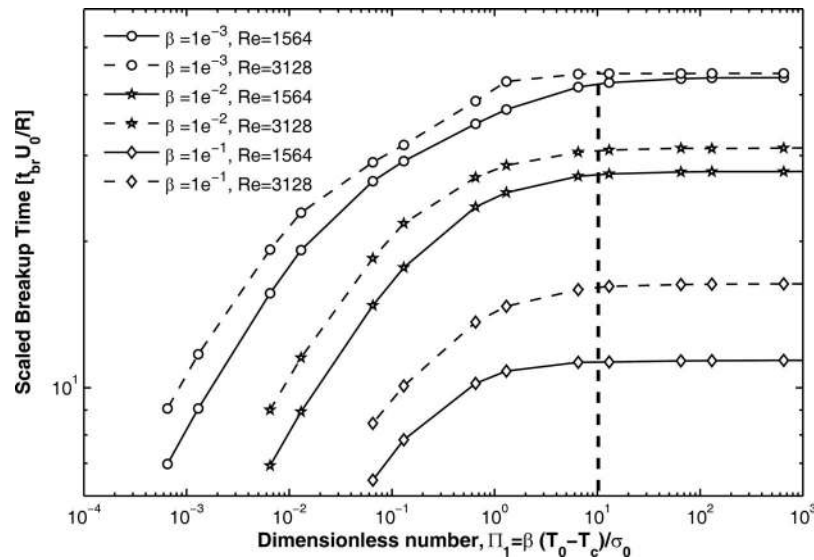


FIG. 16. Breakup time as a function of Π_1 ; presence of a critical Π_1 beyond which Marangoni stress dominates.

F. Non-isothermal spatial analysis with thermally varying surface tension and viscosity—Horizontal jet

The simulations for non-isothermal spatial analysis with thermally varying viscosity and surface tension were carried out for a range of frequencies and the critical frequency that minimizes the breakup time was determined. It was again observed that the critical frequency did not vary with orifice diameters. Also, the critical frequency remained almost the same as that for the isothermal case (Fig. 13). From Fig. 13, it can be seen that the breakup times obtained for this case are slightly larger compared to the case where only surface tension was thermally varying. This is explained based on the fact that viscosity has a damping effect on the growth of perturbations. When heat transfer is taken into account, a decrease in temperature increases the viscosity along the axial length thereby increasing the dampening effect and the breakup time. This also explains why breakup lengths observed are marginally larger for this case (Fig. 15).

VI. CONCLUSIONS

The effect of heat transfer on the breakup of a viscous liquid jet was numerically analysed using the slender jet approximation. It was found that the breakup length was shorter when heat was transferred convectively from the jet to the ambient as compared to isothermal conditions. This is attributed to the increase in surface tension induced by heat transfer. An increase in viscosity with heat transfer, however, is found to have no significant effect on the breakup dynamics. Furthermore, the effect of temperature dependence of viscosity and surface tension did not affect the drop size.

It was found that there exists a critical dimensionless number ($\Pi_1 \sim 10$) which marks the transition between capillary and Marangoni dominated breakup. It was found that beyond the critical number, the breakup length remained independent of Π_1 and was dependent solely on the surface tension gradient, thus indicating that the breakup was dominated by Marangoni stresses. Below the critical number, the jet breaks up due to the combined effects of capillary force and Marangoni stresses.

Experiments were performed with breakup of molten Woods metal in water. It was found that the experimentally observed saturation in debris sizes for larger orifice diameters was captured when the effect of gravity was included. For larger diameters, secondary breakup of the droplets results in a larger spread in the size distribution of debris. However, the theoretical model used

here does not predict secondary breakup behaviour. The results of this work are of significance in safety evaluation during a CDA in a nuclear reactor. Also, an accurate estimation of breakup length assumes significance in design of thermally modulated inkjet printing.

- ¹ J. Eggers, "Nonlinear dynamics and breakup of free-surface flows," *Phys. Rev. Lett.* **71**, 3458 (1997).
- ² Lord Rayleigh, "On the instability of jets," *Proc. London Math. Soc.* **10**, 4 (1878).
- ³ C. Weber, "Zum zerfall eines flüssigkeitsstrahles," *Z. Angew. Math. Mech.* **11**, 136 (1931).
- ⁴ S. Chandrasekhar, *Hydrodynamic and Hydromagnetic Stability* (Oxford University Press, New York, 1961).
- ⁵ S. Tomotika, "On the stability of a cylindrical thread of a viscous liquid surrounded by another viscous fluid," *Proc. R. Soc. London* **150**, 322 (1935).
- ⁶ B. J. Meister and G. F. Scheele, "Generalized solution of the tomotika stability analysis for a cylindrical jet," *AIChE J.* **13**, 682 (1967).
- ⁷ J. B. Keller, S. I. Rubinov, and Y. O. Tu, "Spatial instability of a jet," *Phys. Fluids* **16**, 2052 (1973).
- ⁸ S. J. Leib and M. J. Goldstein, "The generation of capillary instabilities on a liquid jet," *J. Fluid Mech* **168**, 479 (1986).
- ⁹ A. S. Utada, A. Fernandez-Nieves, J. M. Gordillo, and D. A. Weitz, "Absolute instability of a liquid jet in a coflowing stream," *Phys. Rev. Lett.* **100**, 014502 (2008).
- ¹⁰ I. Vihinen, A. M. Honohan, and S. P. Lin, "Image of absolute instability in a liquid jet," *Phys. Fluids* **9**, 3117 (1997).
- ¹¹ J. Eggers and T. F. Dupont, "Drop formation in a one-dimensional approximation of the Navier-Stokes equation," *J. Fluid Mech.* **262**, 205 (1994).
- ¹² E. P. Furlani and M. S. Hanchak, "Nonlinear analysis of the deformation and breakup of viscous microjets using the method of lines," *Int. J. Numer. Methods Fluids* **65**, 563 (2011).
- ¹³ B. S. Cheong and T. Howes, "Capillary jet instability under the influence of gravity," *Chem. Eng. Sci.* **59**, 2145 (2004).
- ¹⁴ E. P. Furlani, "Instability of viscous microjets with spatially varying surface tension," *J. Phys. A* **38**, 263 (2005).
- ¹⁵ E. P. Furlani, B. G. Price, G. Hawkins, and A. Lopez, "Thermally induced Marangoni instability of liquid microjets with application to continuous inkjet printing," *Proc. NSTI Nanotechnol.* **2**, 534 (2006).
- ¹⁶ E. P. Furlani, "Thermal modulation and instability of Newtonian liquid microjets," *Proc. NSTI Nanotechnol.* **1**, 668 (2005).
- ¹⁷ Y. Abe, E. Matsuo, T. Arai, H. Nariai, K. Chitose, K. Koyama, and K. Itoh, "Fragmentation behavior during molten material and coolant interactions," *Nucl. Eng. Des.* **236**, 1668 (2006).
- ¹⁸ Sa. Kondo, K. Konishi, M. Isozaki, S. Imahori, A. Furutani, and D. J. Brear, "Experimental study on simulated molten jet-coolant interactions," *Nucl. Eng. Des.* **155**, 73 (1995).
- ¹⁹ Y. Abe, T. Kizu, T. Arai, H. Nariai, K. Chitose, and K. Koyama, "Study on thermal-hydraulic behavior during molten material and coolant interaction," *Nucl. Eng. Des.* **230**, 277 (2004).
- ²⁰ K. H. Bang, M. K. Jong, and D. H. Kim, "Experimental study of melt jet breakup in water," *J. Nucl. Sci. Technol.* **40**, 807 (2003).
- ²¹ E. Matsuo, Y. Abe, K. Chitose, K. Koyama, and K. Itoh, "Study on jet breakup behavior at core disruptive accident for fast breeder reactor," *Nucl. Eng. Des.* **238**, 1996 (2008).
- ²² A. Passerone, R. Sangiorgi, and G. Caracciolo, "The surface tension of liquid lead," *J. Chem. Thermodyn.* **15**, 971 (1983).
- ²³ J. P. Holman, *Heat Transfer*, 9th ed. (McGraw Hill, 2002).
- ²⁴ H. A. Kuhn, W. F. Hughes, and E. W. Gaylord, "Measurements of the viscosity of liquid Wood's metal," *Br. J. Appl. Phys.* **13**, 527 (1962).